Electronic Supplementary Material (ESI) for Nanoscale Horizons.

Electronic Supplementary Information

Neuromorphic behaviour in discontinuous metal films

Saurabh K. Bose[a], Joshua B. Mallinson[a], Edoardo Galli[a], Susant K. Acharya[a], Chloé Minnai[b], Philip J. Bones[c], and Simon A. Brown[*a]*

[a] The MacDiarmid Institute for Advanced Materials and Nanotechnology, School of Physical and Chemical Sciences, University of Canterbury, Christchurch, New Zealand [b] Molecular Cryo-Electron Microscopy Unit, Okinawa Institute of Science and Technology Graduate University, 1919-1 Tancha, Onna-son, Kunigami-gun, Okinawa, Japan [c] Electrical and Computer Engineering, University of Canterbury, Private Bag 4800, Christchurch 8140, New Zealand

1 Supplementary Information I: Supplementary Figures

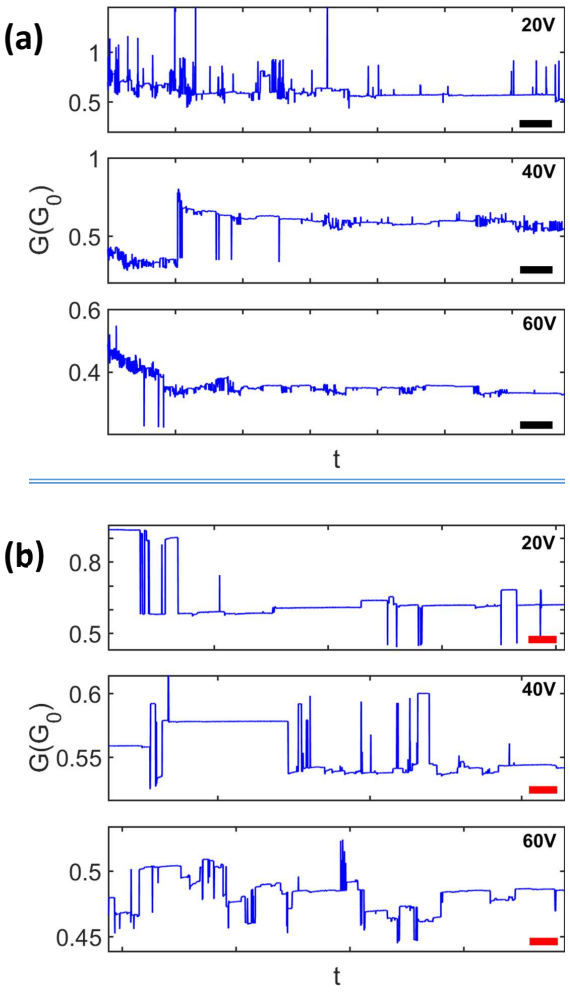

Fig. S1 Stable switching over long periods of time. (a) Switching behaviour measured at 5 Hz sampling rates, over extended time periods ($>$ 200 hrs shown here for device C) with voltage stimuli of V_{app} = 20V, 40V and 60V DC. The scale bars represent 5 hrs. The device is mostly in the high G state throughout this period, with few large switching events to the low G state. (b) Zoomed in snapshots (scale bars represent 2 mins), one for each panel from a, show the step-like switching behavior similar to that observed in nanoparticle networks[1–3]. See main text for details.

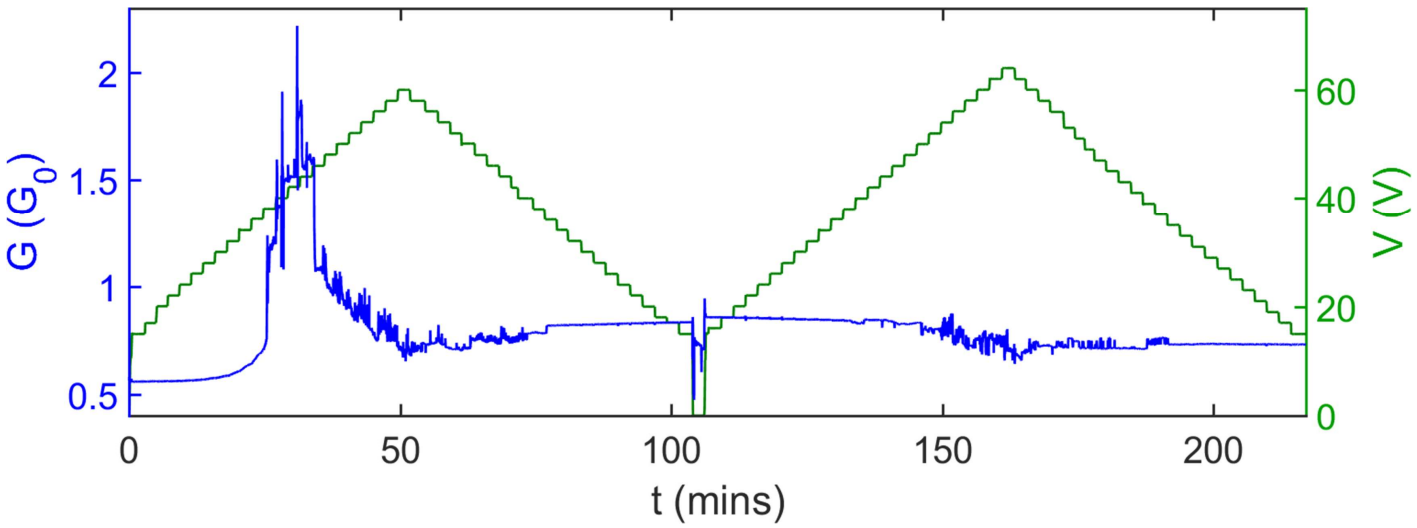

Fig. S2 Voltage dependence of switching. The evolution of conductance switching in Device D is investigated by increasing the applied voltage in steps. During the first sequence (0-100 mins), forming behaviour is observed at $\sim$ 20 min. Vigorous switching is observed at higher voltages during the first sequence. A lower rate of switching is observed (100-225 mins) during the second and subsequent sequences.

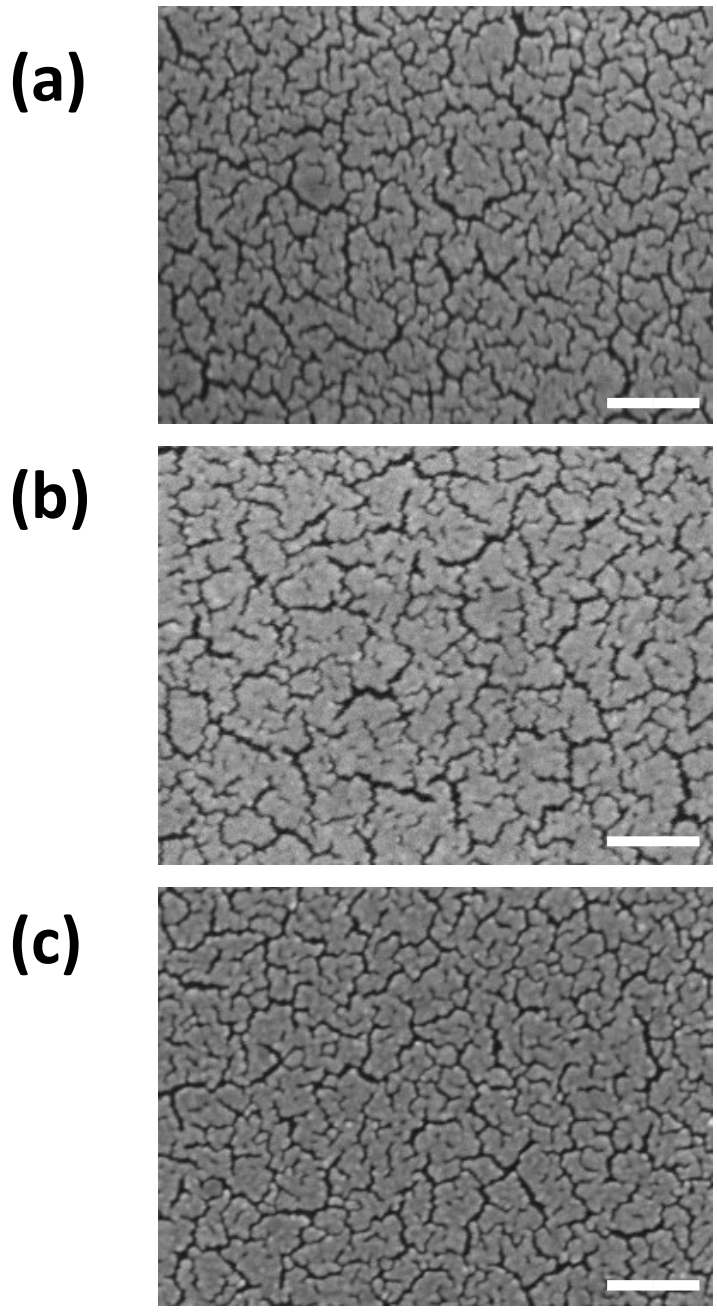

Fig. S3 (a - c) Comparison of the microstructure for three discontinuous Au devices with $R_{dep} \sim 200$ kΩ. All devices showed long-term switching behavior. The scale bars are 200 nm.

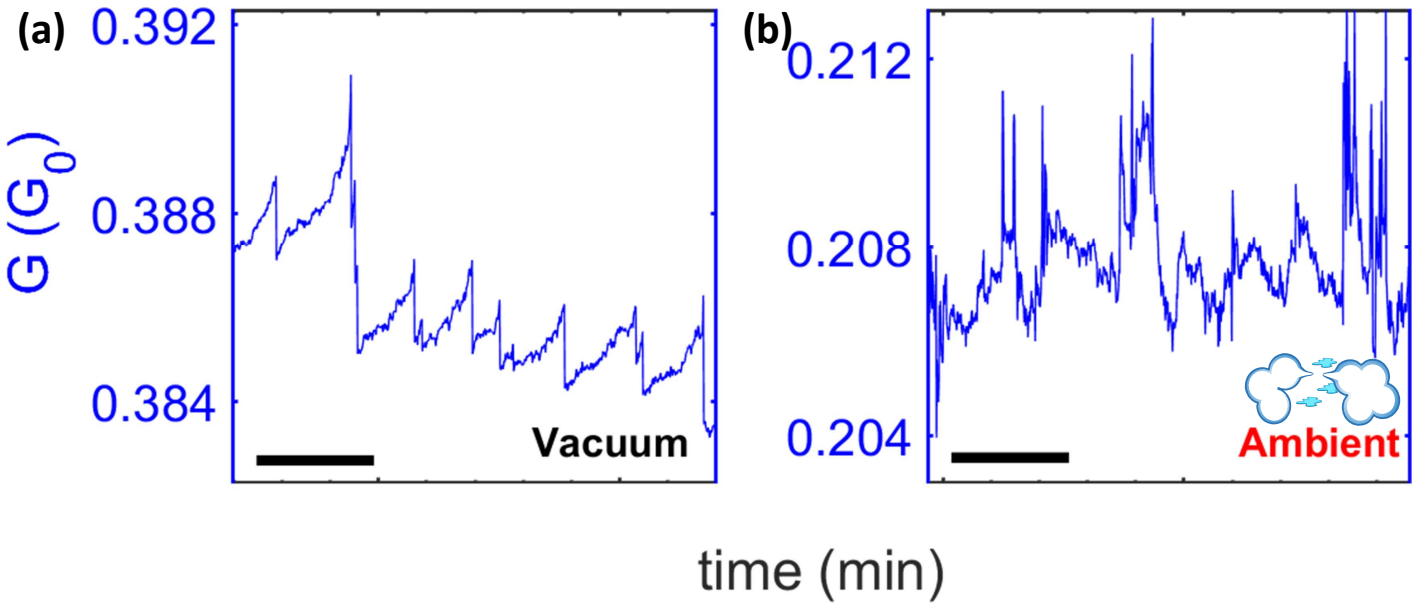

Fig. S4 Effect of ambient atmosphere on conductance switching. To understand the sensitivity of the switching mechanism to ambient conditions Device F was cycled between vacuum and ambient conditions with continuous measurements. (a) In the vacuum typical switching characteristics shown are similar to the low G state characteristic shown in Fig. S7a. Since Device F was deposited at a slightly lower resistance ($R_{dep} \sim 100k\Omega$), the low G state is around $G \sim 0.4G_0$. (b) When the device is exposed to air the switching behaviour becomes 'noisier' and it is more difficult to identify typical switching events. This data is consistent with the formation of well-defined atomic scale filaments in vacuum, whereas in ambient the presence of oxygen and water vapour mean that filaments are likely to have more complex structures and/or that oxidation of the Au surface becomes important due to the high electric fields present in tunnel gaps.[4] The scale bars correspond to 30 s in both the panels.

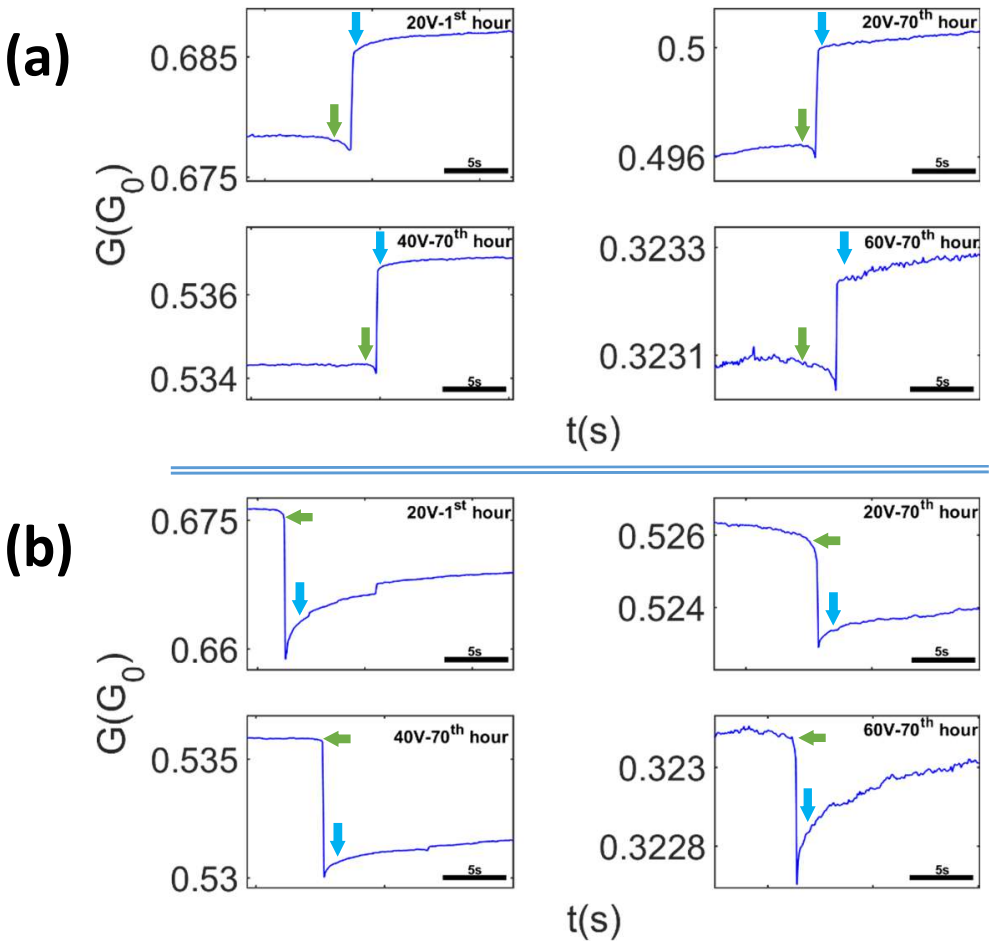

Fig. S5 Snapshots of events from Figure S1a that exhibit continuous changes in conductance. Large events are typically observed as purely stepwise changes in G but many smaller switching events are both preceded (green arrows) by continuous decreases in G and followed (blue arrows) by continuous increases in G. The device is in the high G state for all these events. (a) Examples of increases in G. (b) Examples of decreases in G. See main text and Supplementary Information Section III for details.

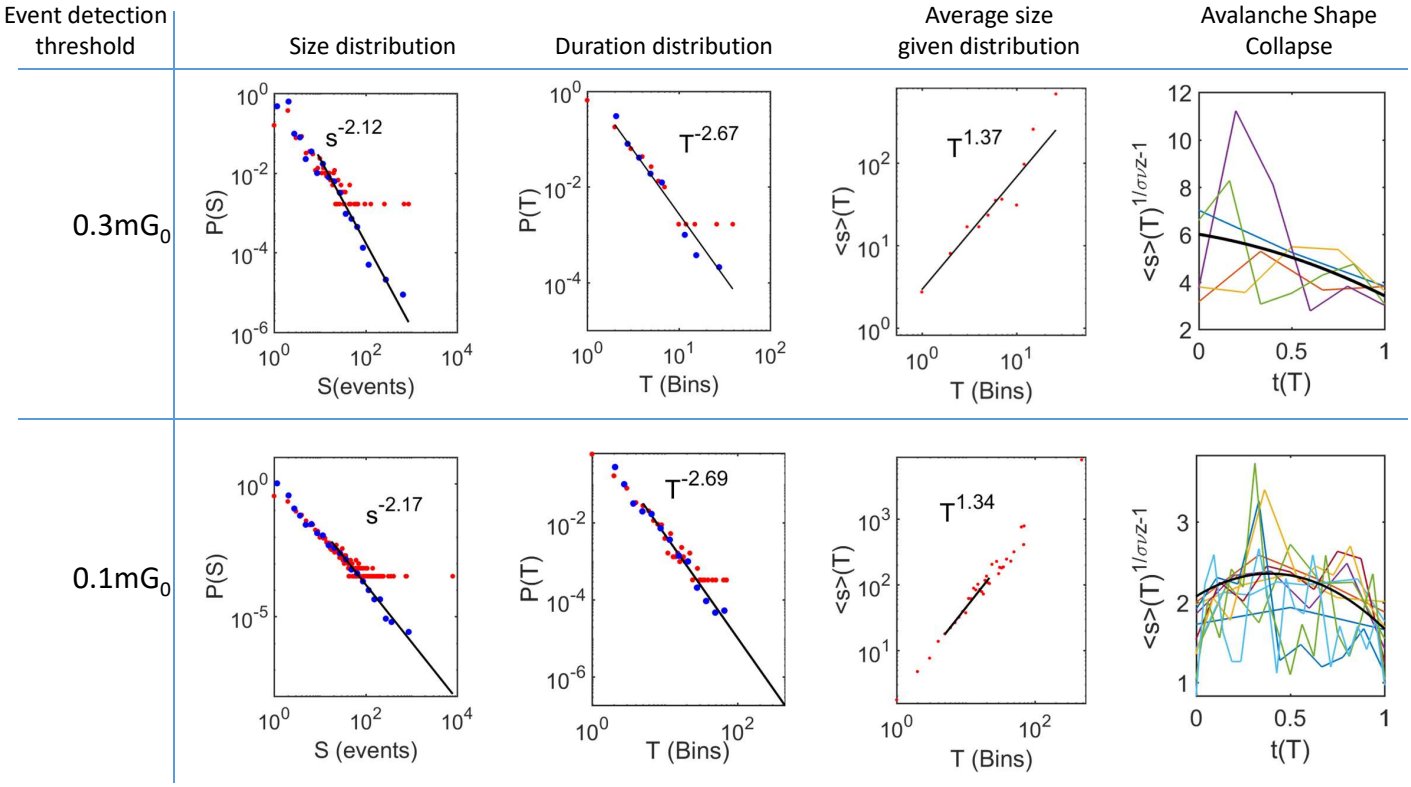

Fig. S6 Avalanche and criticality analysis for a comprehensive dataset from Device C. Sizes (S) and durations (T) of the avalanches as well as the average avalanche size for given duration $< S > (T)$ are distributed as power laws. The plots remain nearly unchanged when the threshold is varied within the plausible range (from 0.3 mG_0 to 0.1 mG_0 – compare top and bottom rows). These histograms require enormous number of avalanches but even with measurements continuing over many days the statistics in the avalanche shape collapse plots are still insufficient to allow a definitive conclusion. The avalanche shape collapse for the lower threshold is nevertheless reasonably good with $1/\sigma\nu_z \sim 1.32 \pm 0.08$. See Table S2 for a comparison of exponents and criticality analysis. The bin size is the average IEI, which is 1.1 s for the top row and 0.2 s for the bottom row.

Exponents	IEI slope	ACF slope	τ	α
Mallinson et al.[2]	1.39 ± 0.01	0.19 ± 0.01	2.01 ± 0.1	2.66 ± 0.1
DF ($\Delta G_{thresh} = 0.3$ mG_0)	1.18 ± 0.01	0.34 ± 0.02	2.1 ± 0.1	2.7 ± 0.1

Table S1 Comparison of DF and Sn nano-cluster devices[2] for IEI and ACF exponents as well as the avalanche exponents (τ, α).

Exponents	τ	α	Crackling relationship	$< S > (T)$	Shape collapse
$\Delta G_{thresh} = 0.3$ mG_0	2.1 ± 0.1	2.7 ± 0.1	1.5 ± 0.2	1.37 ± 0.26	1.04 ± 0.3
$\Delta G_{thresh} = 0.1$ mG_0	2.2 ± 0.1	2.7 ± 0.1	1.5 ± 0.1	1.33 ± 0.06	1.32 ± 0.08

Table S2 Avalanche and criticality analysis for the data shown in Figure S6 (0.3 mG_0 threshold, top row; 0.1mG_0, bottom row). The critical exponent $1/\sigma\nu z$ is obtained from the crackling relationship $(\alpha-1)/(\tau-1)$, mean avalanche size given duration $< S >$ (T), and avalanche shape collapse for both event detection thresholds. Agreement of these three independent estimates of $1/\sigma\nu z$ is a rigorous requirement for criticality.[2,5] Uncertainties are one standard deviation.

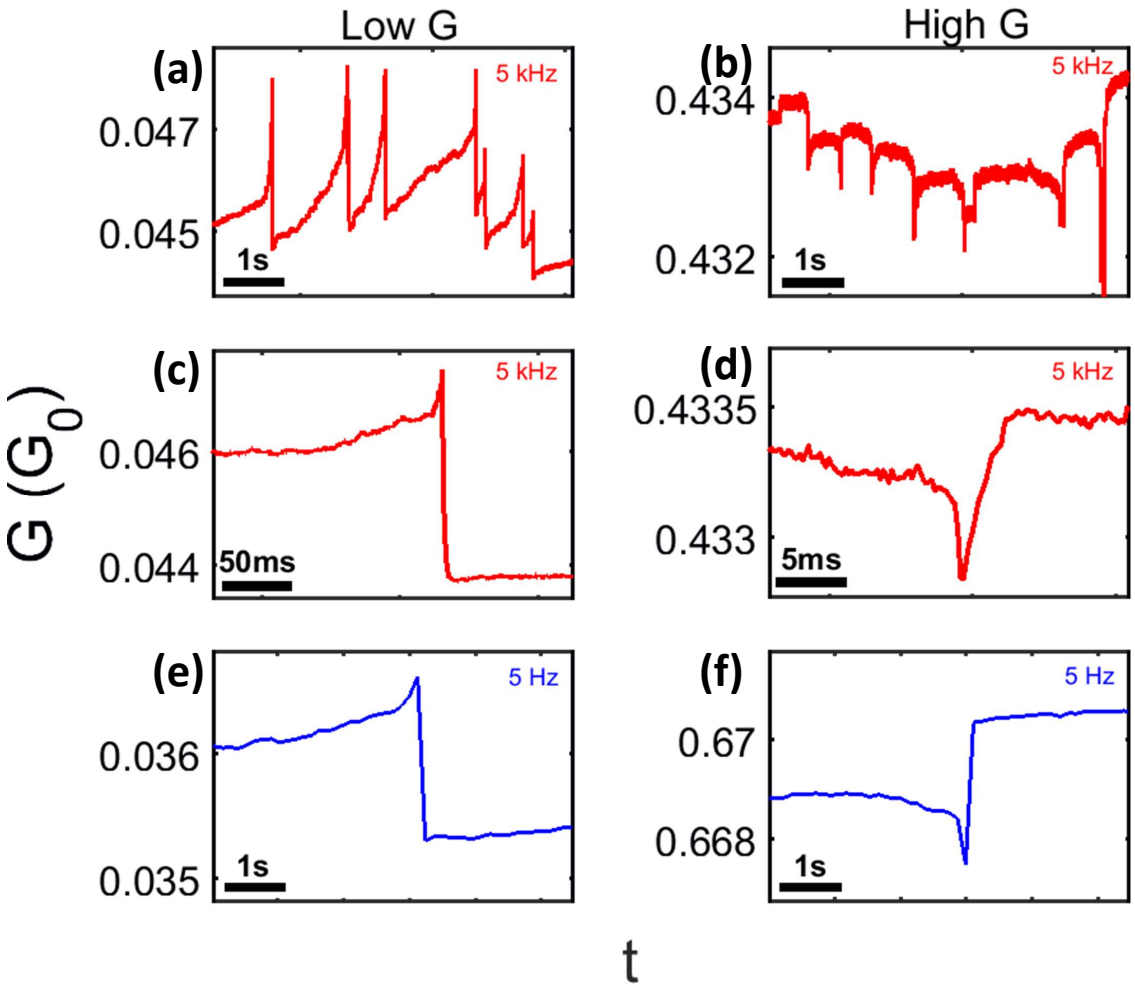

Fig. S7 Distinct switching behaviour in low and high G states. (a,c) In the low G state gradual increases in G due to electric-field induced filament formation in a tunnel gap are followed by sharp decreases in G due to electromigration induced filament breaking. (b, d) In the high G state decreases in G are followed by increases in G. Note the different time scales in c and d *i.e.* 50 ms and 5 ms respectively. (e, f) Similar behaviour to b and d, measured at slower sampling rates. As discussed in the main text and Supplementary Information Section III, these changes are due to the same filament-formation and destruction processes. The data (from Device E) was obtained with both 5 kHz (fast) sampling rates (a-d – red) and with 5 Hz (slow) sampling rates (e,f – blue).

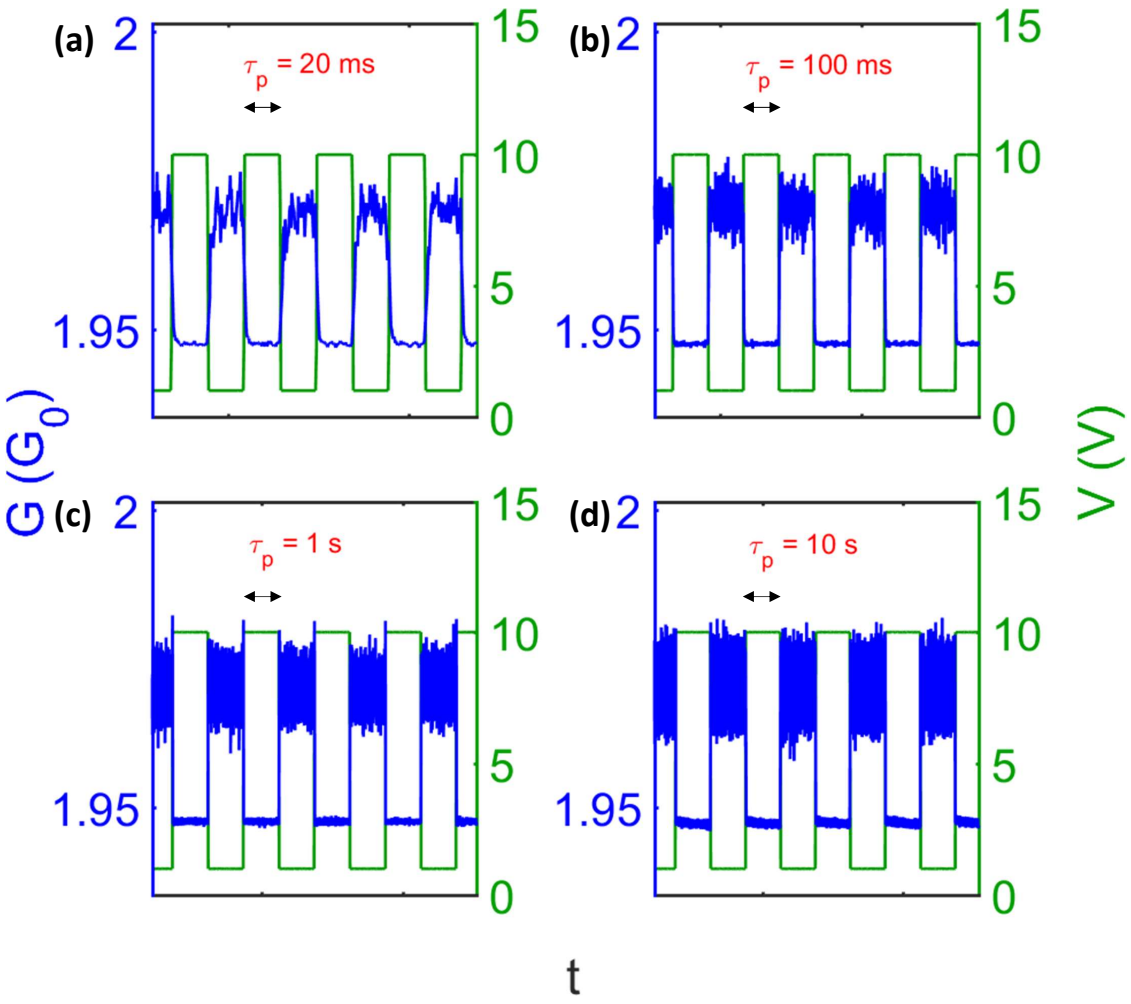

Fig. S8 Investigation of Joule heating at faster sampling rates (5 kHz). For Device B, we performed measurements with voltage pulse widths (τ_p) ranging from 20 ms to 10s. (a-d) The panels show the independence of the measurements on τ_p, demonstrating that the conductance changes are associated with intrinsic $G(V)$ behaviour and not extrinsic effects such as Joule heating. Detailed investigations have shown that capacitive time constants are much shorter than τ_p (*i.e.* $\tau_{RC} \sim 100\ \mu$s).

2 Supplementary Information II: Measurement of $G(V)$ curves.

When the devices are under normal operation (for example with constant DC stimulus, as in Figures 1-3 in the main text) switching occurs often, as filaments are formed and broken in the many tunnel gaps within the film. The switching events can lead to large changes in conductance, and it is therefore not straightforward to measure $I(V)$ curves in both the high and low G states of the devices. This section describes a procedure that was developed in order to capture $I(V)$ curves in both states, in order to support the numerical modelling described in the next section.

Figure S9a shows the activation of a different sample (device B) to that shown in Figure 1 (main text), using a slightly different sequence of applied voltages and subsequent large switching events between a high conductance state ($G \sim 2G_0$, where $G_0 = 2e^2/h$) and a low conduction state ($G \sim 0.1G_0$). Note that in this example the forming process happens to end with the device in the high G state but similar behaviour is observed in all devices (the precise values of the conductances of the two states vary somewhat). In this example the activation procedure was repeatedly paused in order to measure current-voltage ($I(V)$) characteristics, which were then converted to conductance-voltage ($G(V)$) curves in order to highlight nonlinearities. During this sequence the applied voltage was reduced several times in attempts to 'trap' the device in the low G state (*i.e.* to avoid switching back to the high G state – more detail is shown in Figure S10). Figures S9b,d show that in the low G state (both prior to activation and post activation) the $G(V)$ curves are approximately linear, with a modest increase in conductance at 10 V (this corresponds to a slight nonlinearity in the $I(V)$ curves). However Figure S9c shows that in the high G state the $G(V)$ curves are approximately parabolic, with a *decrease* in conductance. Similar behaviour has been observed previously in metallic DFs, but the physical origin has not been unambiguously identified (see Ref. 6 and refs therein). These non-linearities provide important input to the modelling discussed below.

It is important to note that the $G(V)$ curves show no dependence on the rate at which the applied voltage is ramped (Figure S11). This means that both hysteresis / memory effects and Joule heating can be ruled out. Hysteresis (in the sense that the measured conductance reflects the history of the inputs, resulting in 'figure of 8' $I(V)$ curves and asymmetric $G(t)$ curves as in typical memristors) is clearly absent in the data. Also, the low voltage conductance is constant during the sequence of pulsed inputs (Figure S8) indicating that the state of the device does not change unless switching occurs (furthermore, in the absence of inputs above a threshold voltage, the devices remain in the same state and the conductance is unchanged for periods of days and even weeks). Joule heating would be expected to cause larger conductance changes for the slower voltage ramps in Figure S11. Hence the $G(V)$ data reflect the *intrinsic* voltage dependence of the conductivity of the device, as required for the model discussed in the next section.

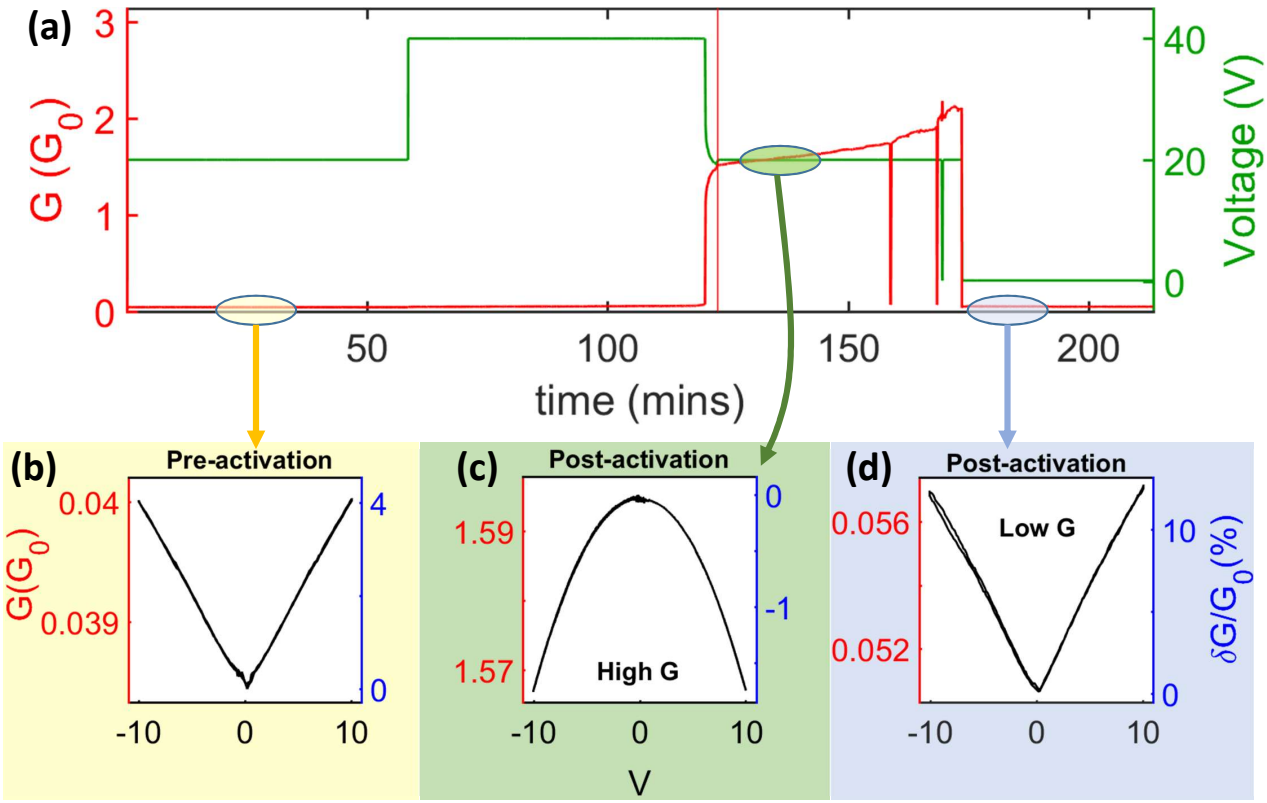

Fig. S9 Voltage dependence of conductance in different network states. (a) Application of 20V and 40V DC to device B resulted in the activation (forming behaviour) after $\sim$ 125 mins with a transition to the high G state ($G \sim 1.6G_0$) and subsequent switching behaviour. Changes in applied voltage are attempts to 'trap' the device in the different states so that $G(V)$ curves can be measured – see Figure S10 for detail. (b) Voltage dependence of conductance $G(V)$ before activation. (c and d) Post activation $G(V)$ in high and low G states respectively. Right axes show the percentage change in G i.e δG / G_0 in each case. Increases in G with V originate from voltage dependence of the tunnel gaps in the network. In the high G state G decreases with V.

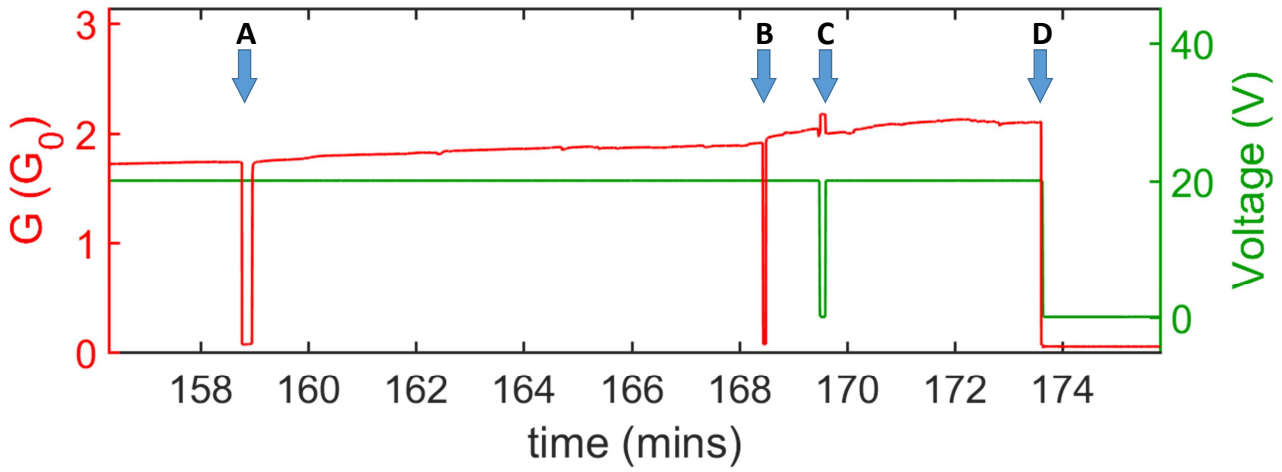

Fig. S10 Attempts to trap a device in the low G state so that low voltage $I(V)$ curves could be obtained in that state. 20V DC was applied to Device B and the conductance measured over time. At $t \sim 159$ mins, the device switched to the low G state (arrow A), but no attempt to turn off the voltages was made. Another transition to the low G state occurred at $t \sim 168$ mins (arrow B) but the applied voltage was not decreased quickly enough (arrow C) and the device returned to the high G state. Finally at $t \sim 173.5$ mins (arrow D) the voltage was successfully lowered to 0.1V just after the device switched to the low G state. Subsequent $G(V)$ measurements in the low G state were performed using $V <$10V to avoid switching back to the high G state.

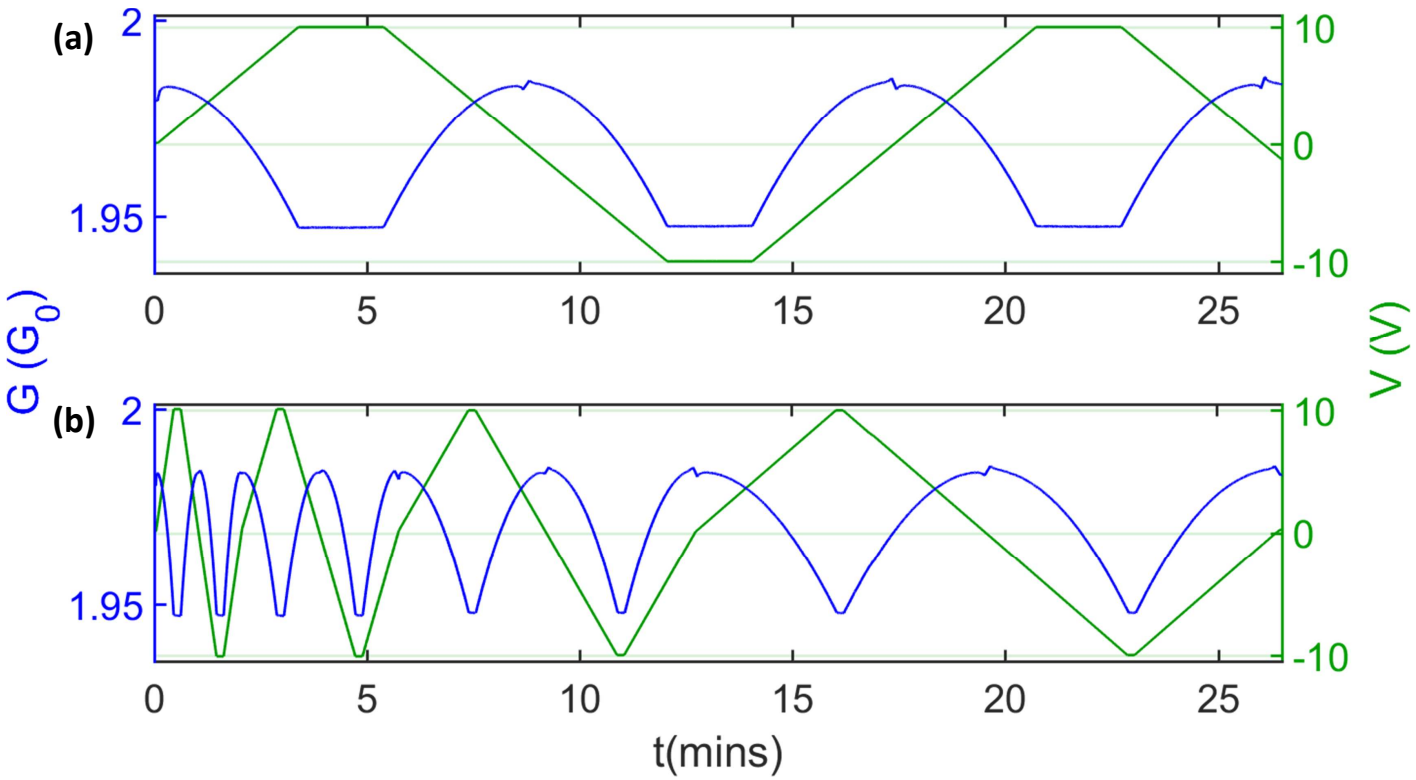

Fig. S11 Investigation of Joule heating. With the Device B in high G state, the voltage was swept between $\pm$ 10 V at different rates. The absence of any change in the maximum G indicates that the decreases in G with V are an intrinsic property of the highly connected DFs and demonstrate that the $G(V)$ behavior is not caused by extrinsic effects such as Joule heating.

3 Supplementary Information III: Numerical simulations of the switching behaviour in discontinuous films

In order to explain the interesting inverted conductance behaviour in the high G state (examples shown in Figures S5 and S7, and summarised in Figure S12 – compare panels e and g), we model the complex percolating network as a simple circuit in which a single active tunnel gap (hillock formation takes place in this tunnel gap) is located between two well-connected groups of nanoparticles (groups A and B in Figure S12a-c) which have high conductance. A third well-connected group, C, is connected to A by a second (lower) tunnel gap which acts as a switch. When the lower switch is closed, the network is in the high G state because group C provides an additional parallel path to ground. When the lower switch is open the network is in the low G state because almost all the current has to flow through the upper tunnel gap (it has higher conductance than the lower gap, but its conductance is still orders of magnitude lower than when a filament is formed). To simplify the argument we ignore any time dependence of the conductance of the lower tunnel gap (due to hillock formation) and treat it as a simple switch. Note that the same model / equivalent circuit can be applied regardless of which tunnel gaps / switches in the real (much more complex) network are active.

The well-connected groups A, B, C each have high conductance and so these individual groups exhibit strong $G(V)$ behaviour that is similar to that observed in the high conductance state of the network as a whole. [The conductance of any square within a homogeneous square network is the same as the conductance of the network. While a percolating network may not be completely homogeneous, this is still a reasonable assumption for large networks.] To reduce the number of free parameters, we assume that the 3 groups A, B and C are identical (*i.e.* both the conductances and their voltage dependences are identical). This is obviously an oversimplification but, as is shown below, this is sufficient to explain the interesting inverted conductance behaviour. A more sophisticated model in which A, B and C have different conductances and voltage dependences allows a closer match to the experimentally measured values of changes in conductance during hillock formation, but is less satisfying because of the large number of parameters.

The effect of the equivalent circuit was modelled numerically, as shown in Figure S12h-k. The conductance of the tunnel gap is modelled using the standard equation[7]:

$$G = \gamma V^2 + \beta \tag{1}$$

where β represents the zero bias conductance and a positive γ generates a voltage-dependent increase of the conductance as the bias reduces the effective height of the tunnel barrier. Since the measured $G(V)$ curves in the high G state are parabolic (Figure S12f) we use the same equation to model the highly connected parts of the network (A, B, and C). [Note that (i) the chosen values of γ must be negative to reproduce the curvature in Figure S12f and (ii) while the physical origin of this negative curvature is still unknown,

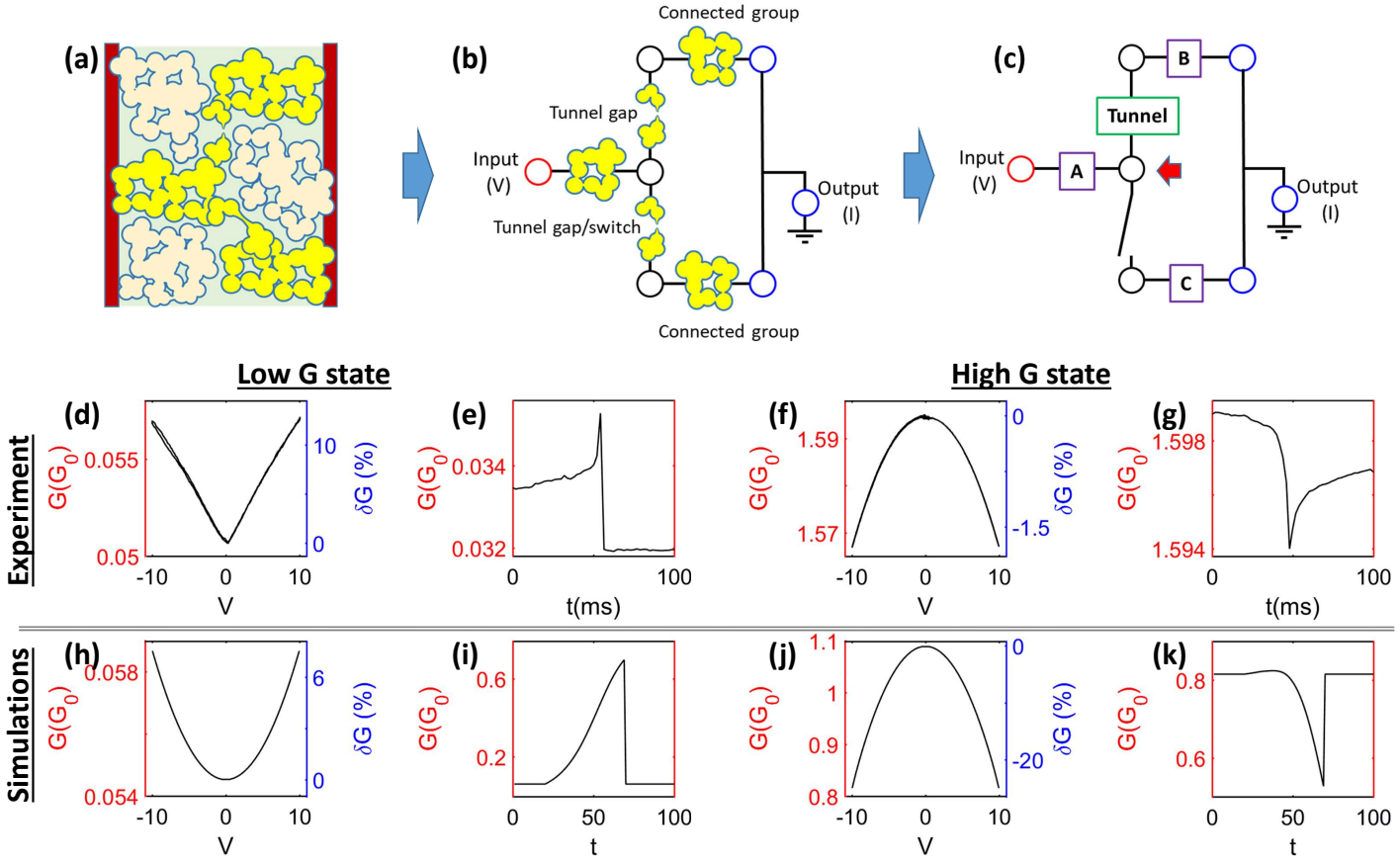

Fig. S12 Reproduction for readers' convenience of Figure 4 from the main text.

it is obviously not tunneling, which yields positive curvature in $G(V)$.] The parameters are chosen to achieve the most satisfactory agreement with the experimental results: for the tunnel gap $\gamma_t = 4 \times 10^{-9}\Omega^{-1}V^2$ and $\beta_t = 4.44 \times 10^{-6}\Omega^{-1}$; for the networks A, B and C $\gamma_N = -1.67 \times 10^{-6}\Omega^{-1}V^2$ and $\beta_N = 1.67 \times 10^{-4}\Omega^{-1}$;

Since the potential across the tunnel gap (V_t) and across the various parts of the network (V_A, V_B, V_C) are dependent on both their own conductances as well as those of the other circuit elements, the solution to Kirchoff's Laws must be found iteratively. At each value of the applied voltage (V) to be considered, the procedure is as follows. We first make an initial estimate of G_t, G_A, G_B, G_C and then use Kirchoff's Laws to calculate the potentials across all the circuit elements in Figure S12c. These potentials are then used to calculate new values for the conductances using equation 1. The potentials are then recalculated and the process continues iteratively until the potentials and conductances all converge. At this point the conductance of the circuit (G) has been determined for a single value of V. We then run the same iterative process for the other applied voltages of interest. $G(V)$ curves can then be plotted, as shown in Figures S12 h and j (for the two cases where the switch (lower tunnel gap) is open and closed respectively). The $G(t)$ curves (Figures S12 i and k) are modelled using a similar iterative process, using a fixed V. The tunnel gap is initially fully open, and then, as it closes, its conductance is increased as an exponential function of time. At each timestep all conductances and voltages are again calculated iteratively until they converge.

The generation of the interesting inverted conductance behaviour due to the effect of the equivalent circuit is explained physically as follows. A voltage is applied, which is distributed across the series/parallel network shown in Figure S12c. The voltage across the upper tunnel gap causes a hillock to grow, and the conductance of the upper tunnel gap increases. In the low G state, the lower switch is open and no current flows through the branch of the network that includes group C, and so the voltage dependence of C is irrelevant. Because the upper tunnel gap has a lower conductance than A or B, almost all the applied voltage is distributed across the upper tunnel gap. Hence the conductance of the network increases as the conductance of the tunnel gap increases due to hillock growth, and the measured voltage dependence for the network (non-linearity in $G(V)$, shown in Figure S12) is that of the upper tunnel gap. Little voltage is distributed across A or B, and so the voltage dependence of A and B are unimportant.

In contrast, when the lower switch is closed (high G state), the voltage across the upper tunnel gap is determined by the more complex series parallel network. The tunnel gap has low conductance, it is the voltage division between A and C that primarily determines the voltage at the point in the circuit indicated with a red arrow in Figure S12c. In our simplified model, A and C are identical and so the voltages across them are similar (because of the tunnel gap, the upper parallel branch of the network through group B has much lower conductance than the lower parallel branch through C and does not significantly affect the distribution of voltages). When the hillock starts to grow in the upper tunnel gap the overall conductance of the parallel part of the network (elements B and C) increases, resulting in a greater voltage drop across A. Because G decreases with V for A this means that the conductance of A decreases, and hence (because A is the chokepoint in the network) the conductance of the network as a whole decreases. Therefore, counter-intuitively, the *increase* in conductance of the upper tunnel gap due to hillock formation leads to a *decrease* in measured conductance for the network as a whole.

Notes and references

[1] A. Sattar, S. Fostner and S. A. Brown, *Physical Review Letters*, 2013, **111**, 136808.

[2] J. B. Mallinson, S. Shirai, S. K. Acharya, S. K. Bose, E. Galli and S. A. Brown, *Science Advances*, 2019, **5**, eaaw8438.

[3] C. Minnai, A. Bellacicca, S. A. Brown and P. Milani, *Scientific Reports*, 2017, **7**, 7955.

[4] R. Aso, Y. Ogawa, T. Tamaoka, H. Yoshida and S. Takeda, *Angewandte Chemie - International Edition*, 2019, **58**, 16028–16032.

[5] N. Friedman, S. Ito, B. A. W. Brinkman, M. Shimono, R. E. L. DeVille, K. A. Dahmen, J. M. Beggs and T. C. Butler, *Physical Review Letters*, 2012, **108**, 208102.

[6] R. P. Barber, S.-Y. Hsu, J. M. Valles, R. C. Dynes and R. E. Glover, *Physical Review B*, 2006, **73**, 134516.

[7] J. G. Simmons, *Journal of Applied Physics*, 1963, **34**, 1793.